http://dx.doi.org/10.5516/NET.09.2014.017

MODAL CHARACTERISTIC ANALYSIS OF THE APR1400 NUCLEAR REACTOR INTERNALS FOR SEISMIC ANALYSIS

JONG-BEOM PARK[1*], YOUNGIN CHOI[1], SANG-JEONG LEE[1], NO-CHEOL PARK[1†], KYOUNG-SU PARK[2], YOUNG-PIL PARK[1], and CHAN-IL PARK[3]
[1]Department of Mechanical Engineering, Yonsei University
50 Yonsei-ro, Seodaemun-gu, Seoul 120-749, Korea
[2]Department of Mechanical Engineering, Gachon University
1342 Seongnamdaero, Sujeong-gu, Gyeonggi-do, 461-701, Korea
[3]Korea Institute of Nuclear Safety
62 Kwahakro, Yuseong-gu, Daejeon 305-338, Korea
[*]Corresponding author. E-mail : pnch@yonsei.ac.kr

Received February 19, 2014
Accepted for Publication April 24, 2014

Reactor internals are sensitive to dynamic loads such as earthquakes and flow induced vibration. Thus, it is essential to identify the dynamic characteristics to evaluate the seismic integrity of the structures. However, a full-sized system is too large to perform modal experiments, making it difficult to extract data on its modal characteristics. In this research, we constructed a finite element model of the APR1400 reactor internals to identify their modal characteristics. The commercial reactor was selected to reflect the actual boundary conditions. Our FE model was constructed based on scale-similarity analysis and fluid–structure interaction investigations using a fabricated scaled-down model.

KEYWORDS : Reactor Internals, Scaled-down Model, Fluid–structure Interaction, Finite Element Method, Commercial Reactor

1. INTRODUCTION

Recently, researchers' interest in seismic design and structural dynamic integrity has been growing in the wake of the radioactive leakages at the Fukushima nuclear power plant. Since an earthquake acts as an external vibration source, it can critically damage reactor internals. Thus, to prevent seismic effects, it is important to accurately analyze the dynamic characteristics of a nuclear reactor.

In this research, we used finite element (FE) analysis. Various FE models have been used to assess the seismic integrity of nuclear reactors. In the past, FE models with one-dimensional beam elements were widely used to reduce the computational time required for seismic analysis. However, a critical disadvantage of a beam model is that it cannot reflect specific boundary conditions or dynamic behaviors. For example, in the one-dimensional model, the reactor vessel (RV) behavior in the x and y directions can be reflected, but it is difficult to consider its behavior in the z direction; that condition can affect the particular modes of a structure. Thus, in this study, we constructed a detailed three-dimensional (3D) FE model to reflect the real model's dynamic behavior more accurately.

In recent years, there have been many reports on the methods that can be used to select the response measurement locations of reactor internals in order to perform modal experiments [1]-[3]. However, such research had the limitation that they considered single components of the reactor internals, and only used analytical methods, making it difficult to determine the exact boundary conditions and characteristics of the completely assembled reactor internals.

To address this weakness, we have previously presented a methodology for identifying the dynamic characteristics, called the **S**ystem-integrated **M**odular **A**dvanced **R**eac**T**or (SMART) [4]-[6].

In the present research, the overall process follows the SMART methodology, but we depart from our previous work by considering APR1400, a currently operating commercial reactor. The APR1400 is a Korean nuclear reactor designed to meet more stringent safety standards, including severe accident mitigation; to secure a stable energy supply; and to advance existing nuclear power technology [7]. This is the first time the SMART methodology has been adjusted for application to commercial reactor internals. Exact boundary conditions are the most

important parts of the scale-similarity analysis. However, in our previous research, it was difficult to clearly express the boundary conditions in a scale-similarity analysis because SMART was not a commercial reactor. For example, we could not consider the supporting conditions of the RV, so we fixed the entire lower surface of the RV to the base surface plate. However, we were able to manufacture support fixtures in this research because we knew the exact supporting condition of the RV. The resulting differences in the boundary conditions lead to considerably different dynamic characteristics. Thus, this research has the great advantage of analyzing dynamic characteristics based on exact boundary conditions.

The main purpose of this study is to construct an FE model that can be used for seismic analysis based on modal tests and FE analysis and which exploits the emerging features of next-generation nuclear power plants. In order to use the FE model for seismic analysis, it is essential to reflect the characteristics of the real model. Thus, by manufacturing a scaled-down model of the commercial reactor internals and carrying out modal experiments on it, we determined the dynamic characteristics of the scaled-down model. We then constructed the FE model with these characteristics in mind. Then, by applying scale-similarity relations, we constructed an FE model that reflected the characteristics of the full-scale model.

2. IDENTIFICATION OF REACTOR INTERNALS' DYNAMIC CHARACTERISTICS

2.1 Description of the APR1400 Internals

The RV assembly in the APR1400 consists of a vertical cylindrical shell, a hemispherical lower head, and a hemispherical upper head (Fig. 1). The reactor internals comprise the core support barrel (CSB) assembly and the upper guide structure (UGS) assembly. Each of these structures has a low-frequency bending mode, since they each have a high slenderness ratio. When the structures interact with the reactor coolant, a fluid–structure interaction (FSI) effect occurs, reducing the natural frequencies of the structures. Since earthquake inputs are generally of low frequency, the bending frequencies of these two structures are of paramount importance in the prevention of seismic hazards.

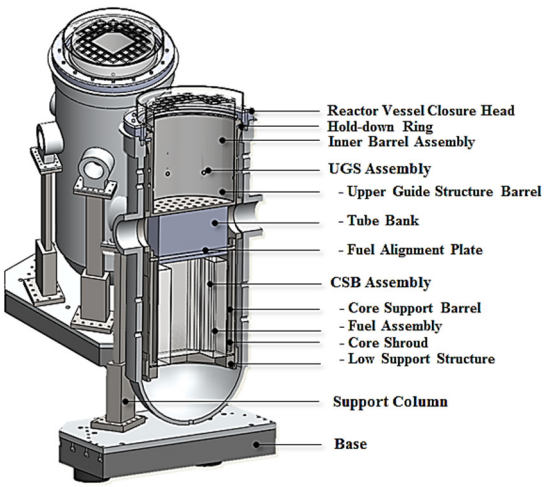

Fig. 1. Schematic of the APR1400 Reactor Internals

2.2 Modal Analysis using a Scaled-down Model

It is essential to obtain valid dynamic characteristics of a system in order to construct a useful FE model. However, it is difficult to identify the dynamic characteristics of a full-sized model including FSI, because dynamic tests cannot be performed on a full-sized model in a laboratory. Accordingly, a scaled-down model was constructed for this study.

An advantage of a scaled-down model is that it enables exact determination of the added-mass effect by comparing the results of modal tests in air and in water. Another advantage is that it allows experiments to be performed by using light materials and small structures. Also, it allows the dynamic characteristics of the actual system to be calculated via scale-similarity analysis.

We constructed a 1/10-scale model of the reactor internals (Fig. 2). In general, the 1/10 scale ratio for reactor internals is recommended by the Comprehensive Vibration Assessment Program (CVAP). Also, the scale ratio was selected by considering interferences among the reactor internals. By performing a pre-test, we found that 1mm was the minimum gap that did not lead to collisions between the structures; that is to say, collisions could still occur if the gap was smaller than 1mm. Therefore, taking all conditions into consideration, we constructed the scaled-down model to be as similar as possible to the actual model.

The scaled-down model had different dynamic characteristics to a full-scale model due to three causes. As mentioned above, the scaled-down model was designed so as to have uniformly scaled-down geometry. Thus, firstly, this geometry made the structures have high natural frequencies. Secondly, the difference in material properties affected

Fig. 2. Scaled-down Fabricated Model

the dynamic characteristics of the system. Finally, differences in the added-mass effect arise from the differences in FSI at the two scales. In this research, therefore, we focused on preparing a FE model that was based on an accurate scaling of the fabricated model's dynamic characteristics.

The differences in dimensions and material properties between the scaled-down model and the full-scale model can be corrected for by means of scale-similarity analysis. The characteristics of the structures in air vary according to their differences in scale, Young's modulus, and density. Considering these factors, we modified the characteristics of the scaled-down model to accurately reflect the characteristics of the full-scale model.

To facilitate FE analysis and modal testing, our design of the scaled-down model excluded structures for which the natural frequency was outside the frequency range relevant to seismic analysis. The major components for modal analysis were selected based on a preliminary FE analysis.

Actual reactor vessels are made of low-alloy steel, and reactor internals are made of 304 stainless steel, owing to its corrosion resistance. However, the scaled-down model was made of aluminum alloy 6061 to facilitate experimental control.

Hydroelastic vibration analysis of a scaled-down model should be focused on extracting modal data such as natural frequencies, modal damping values, and boundary conditions. Thus, we performed modal experiments in various conditions: on each single component, partially assembled models, and the completely assembled model; and testing each component and assembly both in air and in water. Testing all these conditions was important to extract the exact dynamic characteristics. By performing these experiments, we could reflect the exact boundary conditions and added-mass effects.

The procedure of experiments followed the procedure summarized in Fig. 3. First, a component-level modal analysis was performed. By comparing the results of FE analysis and a modal test in air, it was possible to construct valid FE models of each component. In addition, this allowed observation of the added-mass effect, thereby allowing comparison with modal data in water. Secondly, a modal analysis of the partially assembled models was carried out. In general, connections between the structures reduced the natural frequency. Thus, in this process, it was important to exactly represent the boundary conditions of the scaled-down model when applying them to the FE model. Similar to the modal analysis of single components, modal analysis of the partially assembled model was carried out in water to observe the added-mass effect. Finally, the dynamic characteristics of the completely assembled model were analyzed in air and in water, and the dynamic characteristics of the full-scale model were predicted by means of scale-similarity analysis.

2.3 Experimental Setup

Each single component was tested under free–free conditions to exclude natural frequency reductions due to fixed boundary conditions (Figs. 4a, 4b). In order to create free–free conditions, we used string to suspend the structures. Heavy components and the assembled model were too heavy to be suspended in this way, and were instead placed on cushioning material. The structures were excited by an impact hammer. The responses were measured with accelerometers, and the modal characteristics were extracted by using LMS Test LAB software. An exciter

Modal Analysis In Air	Modal Analysis In Water
Component-level models	**Component-level models**
RV CSB UGS IBA	
Partially Assembled models	**Partially Assembled models**
RV + CSB RV + CSB Assembly RV + UGS Assembly + IBA	RV + CSB Assembly RV + UGS Assembly + IBA
Totally Assembled model	**Totally Assembled model**
RV + CSB Assembly + UGS Assembly + IBA	RV + CSB Assembly + UGS Assembly + IBA

Fig. 3. Hydroelastic Vibration Analysis Procedure

Fig. 4. Experimental Setup for Modal Tests

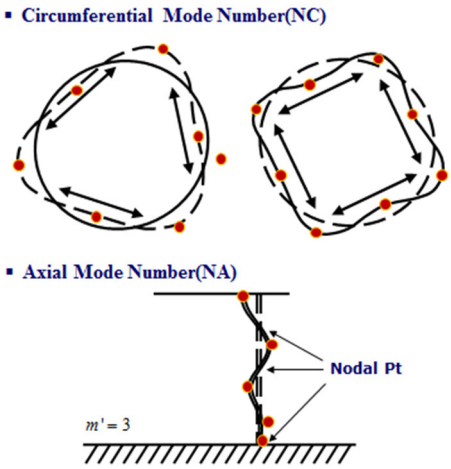

Fig. 5. Particular Mode Shapes for a Cylindrical Shell

was used to excite large-scale structures that could not be excited using an impact hammer, such as the RV and assembled structures; also, all modal experiments in water used the exciter. Figs. 4c and 4e show the excitation modal test; Fig. 4d shows the RV being filled with water to allow investigation of the FSI effect and added-mass effect.

In the modal experiments, excitation and response points were selected based on the mode shapes that were obtained from the preliminary FE analysis. Excitation could be maximized by selecting excitation points that were distant from the nodal points. The response points were selected to allow clear extraction of the shapes of the low-order modes. For example, Fig. 5 shows particular mode shapes for a cylindrical shell; based on these shapes, five axial response points were selected to observe the three nodal points. In the same manner, eight radial response points were selected to examine the case in which the wave number in the radial direction was four. Thus, 96 response points were chosen for the UGS assembly and 112 response points were chosen for the CSB assembly.

3. FINITE ELEMENT METHOD

The coolant in a nuclear reactor plays a dominant role in the reactor's dynamic characteristics. Hence, to construct a valid FE model, it is important to represent FSI and boundary conditions in the model; the present study was focused on these tasks.

3.1 Theoretical Development of the Finite Element Method

3.1.1 Added Mass and Stiffness Effects

Added mass and stiffness effects play significant roles in structures that are submerged in coolant water. Equations (1)-(6) were derived previously [6]. The virtual work for a submerged structure includes not only the kinetic energy of the structure, but also the kinetic energy of the fluid flow, which can be used to represent the virtual mass as follows:

$$M_a = 2T / U^2, \tag{1}$$

where M_a, U, and T denote the added mass, the velocity of the structure, and the kinetic energy, respectively.

The general equation for a fluid–structure interaction problem can be written as:

$$\begin{aligned}[M_s]\{\ddot{x}(t)\}+[C_s]\{\dot{x}(t)\}+\left(\left[K_s\right]+\left[K_p\right]\right)\{x(t)\}\\ =\{f_e(t)\}+\{f_f(t)\}\end{aligned}, \tag{2}$$

where $[M_s]$, $[C_s]$, $[K_s]$, and $[K_p]$ respectively denote the mass matrix, damping matrix, stiffness matrix, and the increment of the pre-stressed stiffness matrix of the submerged structure. $[K_p]$ means the increment of stiffness from added mass and pre-stress from the pressurization of fluid. This term can be omitted in the analysis of a reactor system [8]. The total dynamic load on the structure can be expressed as the sum of the external force $\{f_e(t)\}$ and the hydrodynamic force $\{f_f(t)\}$ on the fluid–structure interface. The hydrodynamic force can be represented as the integral of the fluid pressure $\{P\}$ with respect to the infinitesimal interface area dS, as in Equation (3), using Equation (4) to determine the fluid momentum at the fluid–structure interface. In this equation, $\{N_p\}$ is the approximate shape function for the spatial variation of the pressure, ρ_o is the fluid density, and $\{n\}$ is a unit normal vector for the fluid–structure interface.

The general equation that describes the fluid in the finite element method can be expressed in terms of a pressure-formulated element using the Helmholtz equation, or a displacement-formulated element using elastic theory.

$$\{f_f\} = \int_{\Gamma_s} \{N_p\}^T \{n\} \{P\} dS = -[M_a]\{\ddot{x}(t)\} \tag{3}$$

$$n \cdot \nabla P = \rho_0 n \frac{\partial^2 x(t)}{\partial t^2} \tag{4}$$

Substituting Equation (3) into Equation (2) yields

$$\begin{aligned}\left([M_s]+[M_a]\right)\{\ddot{x}(t)\}+[C_s]\{\dot{x}(t)\}+\left(\left[K_s\right]+\left[K_p\right]\right)\{x(t)\}\\ =\{f_e(t)\}\end{aligned} \tag{5}$$

Thus, the characteristic equation must take into account the added mass due to FSI, which decreases the natural frequencies according to

$$\det\left[\left([K_s]+[K_p]\right)-\omega^2\left([M_s]+[M_a]\right)\right]=0 \tag{6}$$

3.1.2 Gap Fluid Effect

Gap fluid has a considerable effect on the dynamic characteristics. The presence of a small gap decreases the natural frequencies dramatically. In addition, damping increases rapidly with decreasing gap size when the structures

are moving out of phase with one another [9]. Accordingly, the gap fluid effect should be considered for submerged structures.

In our FE model, for example, the gap fluid has a role in coupling the CSB with the UGS. The two coaxial cylindrical shells are coupled strongly. The coupling effect occurs equally in the scaled-down model and the full-sized model. Thus, in the FE modeling procedure, the gap fluid was considered in both the scaled-down model and the full-sized model without discrimination. The only difference between them was that the property of the fluid was modified to represent reactor coolant in the full-scale model after the modeling procedure. Also, the added-mass effect from the gap fluid was considered by introducing a non-dimensionalized added virtual mass incremental (NAVMI) factor.

3.2 Construction of the FE Analysis Model

In this study, ANSYS commercial software was used for the FE analysis. The constructed FE model could be utilized for dynamic characteristic identification and seismic analysis.

FE analysis was carried out as follows. First, by comparing the results from the FE model with the results of a component-level modal test, each of the component models was simplified to reduce the analysis time. Second, the mesh generation was controlled. Third, element types and material properties were assigned.

In this model, we used SOLID45 elements for the structures and FLUID30 elements for the fluid. We have employed two kinds of fluid elements in our research: FLUID30 and FLUID80. FLUID30 elements are used to model the fluid medium and the interface in FSI problems. These elements have eight corner nodes with four degrees of freedom per node, and can be used in conjunction with other 3D structural elements to carry out full harmonic response and full transient method analyses. FLUID80 element is a modification of the 3D structural solid element (SOLID45), and is used to model fluids contained within vessels having no net flow rate. Another fluid element (FLUID116) is available to model fluids flowing in pipes and channels. The FLUID80 element is particularly well suited for calculating hydrostatic pressures and fluid–solid interactions. However, the use of FLUID80 elements entails the calculation of many unnecessary fluid modes; thus, FLUID30 elements are more appropriate for observing the shapes of structures in modal analyses, so they were used in this study.

Hexahedral elements were therefore used to represent pressure-formulated fluid elements that cannot be represented by tetrahedral elements. In order to quadrate the boundary nodes, all elements were represented by hexahedral elements. Our model consisted of 609,952 elements, including solid and fluid elements. The sizes of the mesh elements were defined to allow the mapped mesh to be considered in relation to the slenderness of the structures

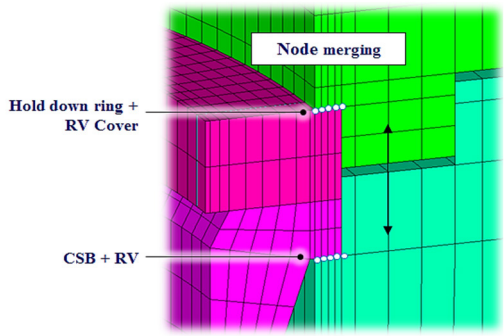

Fig. 6. Control of Boundary Conditions by Means of Node Merging

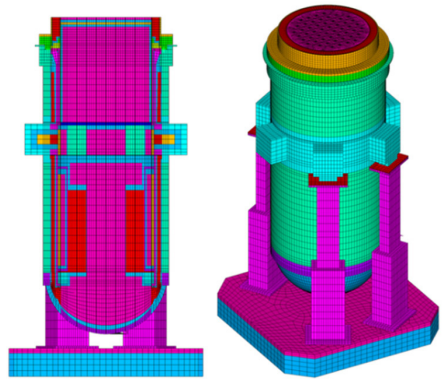

Fig. 7. Finite Element Model of the APR1400 Reactor Internals

and the uniformity of the mesh elements. We confirmed that decreasing the mesh size in this way did not critically affect the resulting dynamic characteristics of our model.

To increase accuracy, the assembled condition of each component was represented via node merging rather than linear bonded contact. In the reactor internals, the upper flange of the core support barrel and the upper guide structure barrel are clamped between the bolted reactor vessels by a hold-down ring. By selecting the number of the merged nodes, we could straightforwardly control the boundary conditions and fluid–structure coupling. For example, as indicated in Fig. 6, five nodes were merged to represent the boundary between the hold-down ring and RV cover. Thus, the clamped region could be expressed by parametric modeling using the ANSYS parametric design language. The completely assembled model included complex fastening conditions between several components. In particular, because bolted conditions reduce the natural frequency, the choice of the number of merged nodes is essential to ensure precise representation. Thus, by tuning the number of merged nodes, we were able to construct a FE model that accurately represented the characteristics of modal experiments.

Finally, using the solver control, we extracted modal properties such as natural frequencies and mode shapes; Fig. 7 shows the FE model constructed considering FSI.

4. SCALE-SIMILARITY ANALYSIS

As discussed above, it is difficult to perform modal experiments on an actual nuclear reactor, and accordingly, we constructed a 1/10-scale model suited to laboratory conditions. The natural frequencies, material properties, and added-mass effect of the scaled-down model are dynamic characteristics that differ from those of the actual nuclear reactor. The differences in these characteristics arise from the different densities and elastic moduli of their different materials. Thus, to properly identify the characteristics of the full-sized model, these three factors should be corrected by means of scale-similarity analysis.

4.1 NAVMI Factor

The added-mass effect varies considerably according to the mode shapes and natural frequencies. Hence, it is necessary to add a NAVMI factor to quantify the added-mass effect with respect to the vibratory mode. The NAVMI factor (Γ) can be represented as follows [10]–[14]:

$$\Gamma = \frac{1}{\zeta_f}\left[\left(\frac{f_O}{f_L}\right)^2 - 1\right] \tag{7}$$

where ζ_f, f_O, and f_L respectively denote the density ratio of water to air, the natural frequencies of the structures in air, and the corresponding natural frequencies of the structures in water.

4.2 Scale Factor and Material Property Correction Factor

The material properties of the scaled-down model can be corrected using the elastic modulus correction factor (ε) and the density correction factor (ζ_p). Equations (15)–(20) below are taken from previous research [6].

$$\varepsilon = \frac{E_r}{E_s} \tag{8}$$

$$\zeta_p = \frac{\rho_r}{\rho_s} \tag{9}$$

Here, E_s, E_r, ρ_s, and ρ_r are the respective elastic moduli and densities of the materials used in the similarity model and in the actual structure. The natural frequency (f_{Om}) of the similarity model with corrected material properties in air can then be written as

$$f_{Om} = \sqrt{\frac{\varepsilon}{\zeta_p}} f_{Os}, \tag{10}$$

where f_{Os} denotes the natural frequency of the similarity model with uncorrected material properties in air. Also,

$$f_{Or} = \frac{1}{\kappa} f_{Om}, \tag{11}$$

where f_{Or} denotes the natural frequency of the full-scale model with correct material properties in air, and κ is a geometric scale factor.

Assuming that the mode shapes in water are equivalent to the mode shapes in air, the NAVMI factor can then be expressed as follows.

$$\Gamma_s = \Gamma_r = \frac{1}{\zeta_s}\left[\left(\frac{f_{Os}}{f_{Ls}}\right)^2 - 1\right] = \frac{1}{\zeta_r}\left[\left(\frac{f_{Or}}{f_{Lr}}\right)^2 - 1\right] \quad \text{with } \zeta_s = \frac{\rho_{Ls}}{\rho_s},\ \zeta_r = \frac{\rho_{Lr}}{\rho_r} \tag{12}$$

Here, Γ_s, Γ_r, ρ_{Ls}, and ρ_{Lr} denote the respective NAVMI factors and fluid densities in the scale-similarity model and in the full-scale model. Combining these equations, the natural frequencies of the full-scale model with different material properties can be obtained as follows:

$$f_{Lr} = \frac{f_{Os}}{\kappa}\sqrt{\frac{\varepsilon}{\zeta_p(1+\zeta_r\Gamma_s)}} = \frac{f_{Os}}{\kappa}\sqrt{\frac{\varepsilon\rho_s}{(\rho_r+\rho_{Lr}\Gamma_s)}}. \tag{13}$$

As indicated by the form of Equation (20), the natural frequencies of a full-scale model that has different material properties than the model can be calculated from the scale factor, material property correction factors, and a NAVMI factor derived from FE analysis or a modal experiment.

5. RESULTS AND DISCUSSION

The results of the modal test were compared with those of the FE analysis. Tables 1–4 give the results for the single-component models and the partially assembled models in air. Tables 5 and 6 give the corresponding results in water, and Table 7 gives the results for the completely assembled model in water. Figure 8 gives the frequency response function of the completely assembled model in water. As can be seen in Table 7, the constructed FE model reflects the dynamic characteristics of the scaled-down model within a valid margin of error.

In general, the vibratory mode (n, m) of a cylindrical shell is distinguished by the number of nodal lines in the axial direction (m) and the wave number in the circumferential direction

Table 1. Natural Frequencies of the RV in Air

Mode Shape (n, m)	Natural Frequencies [Hz]		Error [%]
	FEM	Modal Test	
Rigid body	66	71	7.0
Rigid body	227	214	-6.1
(2,1)	355	360	1.4
(3,1)	604	600	-0.7
(4,1)	1010	961	-5.1

Table 2. Natural Frequencies of the RV + UGS Assembly in Air

Mode Shape (n, m)	Natural Frequencies [Hz]		Error [%]
	Modal Test	FEM	
(1,1)	149	150	0.7
(3,1)	413	420	1.7
(4,1)	688	665	-3.5
(3,2)	792	736	-7.6
(4,2)	880	833	-5.6

(*n*). Because the mode shapes of the CSB were not different when tested in air and in water, these shapes were compared by simply revolving them. These comparisons were confirmed by comparing the vibratory mode number of each of the mode shapes.

The out-of-plane (OOP) and in-plane (IP) modes noted in Tables 7 and 9 indicate the phase differences between the CSB assembly and the UGS assembly. The first bending frequency is about 50 Hz, according to the experimental and FE analysis results given in Table 1. Figure 9a shows the first bending mode shape of the CSB

Table 3. Natural Frequencies of the CSB Assembly in Air

	Mode Shape (n, m)	Natural Frequencies [Hz]		Error [%]
		FEM	Modal Test	
Free–Free Condition	(2, 1)	151	154	1.9
	(2, 2)	217	217	0.0
	(3, 1)	397	374	-6.1
	(3, 2)	511	533	4.1
	(2, 3)	659	641	-2.8
	(3, 3)	708	709	0.1
RV + CSB Assembly	(1, 1)	149	150	0.7
	(3, 1)	413	420	1.7
	(4, 1)	688	665	-3.5
	(3, 2)	792	736	-7.6
	(4, 2)	880	833	-5.6

Table 4. Natural Frequencies of the UGS Assembly in Air

	Mode Shape (n, m)	Natural Frequencies [Hz]		Error [%]
		FEM	Modal Test	
UGS in Free–Free condition	(2, 1)	375	354	-5.9
	(3, 1)	866	824	-5.1
	(4, 1)	1108	1082	-2.4
	(5, 1)	1429	1407	-1.6
	(3, 2)	1586	1616	1.9
	(6, 1)	1911	1885	-1.4
IBA Assembly in Free–Free condition	(2, 1)	72	74	2.7
	(3, 1)	181	181	0.0
	(4, 1)	328	326	-0.6
	(5, 1)	511	508	-0.6
	(6, 1)	737	735	-0.3
RV + UGS Assembly	(1, 1) UGS	362	-	-
	(4, 1) IBA	399	388	-2.8
	(3, 1) IBA	406	-	-
	(5, 1) IBA	538	523	-2.9
	(2, 1) IBA	606	-	-

Table 5. Natural Frequencies of the RV + CSB Assembly in Water

Mode Shape (n, m)	Natural Frequencies [Hz]		Error [%]
	FEM	Modal Test	
(1, 1)	51	55	7.3
(2, 1)	93	73	-27.4
(3, 1)	101	105	3.8
(4, 1)	214	213	-0.5

Table 6. Natural Frequencies of the RV + UGS Assembly in Air

Mode Shape (n, m)	Natural Frequencies [Hz]		Error [%]
	FEM	Modal Test	
(4, 1)	464	485	4.3
(2, 1)	566	525	-7.8
(5, 1)	613	631	2.9

Table 7. Comparison of the Modal Tests and Finite Element Analysis for the Completely Assembled CSB in Water

Mode Shape (n, m)	Natural Frequencies [Hz]		Error [%]
	Modal Test	FEM	
(1,1) OOP	53	50	5.7
(1,1) IP	70	67	4.3
(2,1)	81	71	12.3
(3,1)	108	102	5.6
(4,1)	237	225	5.1
(4,2)	247	252	-2.0

obtained from the experiment. Figure 9b was obtained from the FE analysis. Figure 9c shows the in-phase mode shape of the overall model.

Using scale-similarity analysis, we derived the dynamic characteristics of the full-sized model, which are given in Table 9. The scale-similarity analysis was carried out to the fifth mode in order to validate the FE analysis. The correction factors listed in Table 8 were used to perform

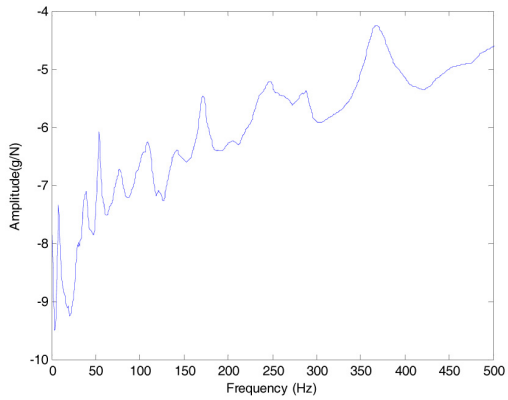

Fig. 8. Frequency Response Function of the Completely Assembled CSB in Water

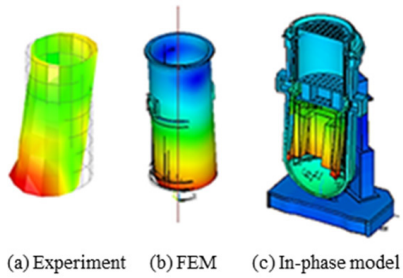

Fig. 9. Bending Mode Shapes of the APR1400 Reactor Internals: Amplitude of Vibration (Acceleration)

Table 8. Correction of Material Properties for the Scale-similarity Analysis

Material Property	Structure			Correction Factor	Fluid	
	Actual Model		Scaled-down Model		Actual Model	Scaled-down Model
	304 Stainless Steel	Low Alloy Steel	Aluminum 6061		Reactor Coolant	Water
Density [kg/m^3]	8000	7850	2700	2.96	744.6	1000
Elastic Modulus [GPa]	200	200	68.9	2.90	-	-
Sound Velocity in Fluid [m/s]	-		-	-	1019.5	1483

Table 9. Results of the Scale-similarity Analysis

Mode Shape (n, m)	Natural Frequencies [Hz]						Factor	
CSB	Scaled-down Model		Actual Model				AVMI	NAVMI
	Air	Water	Air	Reactor Coolant				
				FEM	Calculation	Discrepancy [%]		
(1, 1) OOP	160.1	53	15.8	8.7	8.7	0.0	9.3	25.0
(1, 1) IP	160.1	70	15.8	11.3	10.7	5.3	7.2	19.4
(2, 1)	450.1	81	44.6	13.5	13.5	0.0	16.4	44.2
(3, 1)	457.0	108	45.2	15.6	16.2	-3.8	30.1	81.2
(4, 1)	744.8	237	73.7	38.6	39.4	-2.1	10.0	26.9

the similarity analysis. The materials used in the real model were low-alloy steel for the RV and 304 stainless steel for the other internals. Thus, we considered each material in the FEM. However, in scale-similarity calculation, it is impossible to calculate the NAVMI factor by using three materials: low-alloy steel, 304 stainless steel, and 6061 aluminum. Thus, we calculated the NAVMI factor by using the material properties of 304 stainless steel because we focused on the behaviors of internals in this research.

As Table 9 indicates, the first bending mode of the actual model was 8.7 Hz in water. In Table 9, the 'FEM' row gives the natural frequencies extracted by our FE model, with scales and material properties modified to reflect the full-scale model; the 'Calculation' row gives the natural frequencies calculated based on the NAVMI factor obtained from the experiments on the scaled-down model. The discrepancies between them were less than 5%, thus validating our FE models.

6. CONCLUSION

In this research, we fabricated a 1/10-scale model of the APR1400 reactor internals, carried out modal experiments on the scaled-down model to identify its dynamic characteristics, and used these characteristics to construct a FE model of the full-scale system. Modal experiments in air allowed exact representation of the geometry and the boundary conditions, and modal experiments in water yielded FSI information. Then, scale-similarity analysis was performed to extract the characteristics of the full-scale model. Finally, by comparing the natural frequencies obtained by the FEM and by calculation, we verified the validity of our FE model.

In seismic analysis, we prioritized the first bending mode shape because the frequency of seismic waves is near the first bending frequency of the structure. We subsequently confirmed that the discrepancy was less than 5% between the first frequencies obtained by the FE model and by the calculation based on scale-similarity analysis, validating our model. Thus, we can conclude that our model is suitable for use in future seismic analysis.

REFERENCES

[1] D. Y. Ko, K. H. Kim, and S. H. Kim, "Response instrumentation test acceptance criteria for APR1400 RVI CVAP," *Trans. Korean Soc. Noise Vib. Eng*., vol. 21(11), pp. 1036–1042 (2011).

[2] D. Y. Ko, K. H. Kim, and S. H. Kim, "Structural analysis and response measurement locations of inner barrel assembly top plate in APR1400," *Trans. Korean Soc. Noise Vib. Eng*., vol. 22(5), pp. 474–479 (2012).

[3] D. Y. Ko, K. H. Kim, and S. H. Kim, "Structural analysis and measuring locations of upper guide structure assembly in APR1400," *Trans. Korean Soc. Noise Vib. Eng*., vol. 23(1), pp. 49–55 (2013).

[4] S. H. Lim, Y. I. Choi, K. R. Ha, K. S. Park, N. C. Park, Y. P. Park, K. H. Jeong, and J. S. Park, "Dynamic characteristics of a perforated cylindrical shell for flow distribution in SMART," *Nucl. Eng. Des*., vol. 241, pp. 4079–4088 (2011).

[5] Y. I. Choi, S. H. Lim, B. H. Ko, K. S. Park, N. C. Park, Y. P. Park, K. H. Jeong, and J. S. Park, "Dynamic characteristics identification of reactor internals in SMART considering fluid–structure interaction," *Nucl. Eng. Des*., vol. 255, pp. 202–211 (2013).

[6] S. H. Lim, "Hydroelastic vibration analysis of reactor internals with fluid–structure interaction through scale-similarity model," Dissertation, Yonsei Univ., Seoul, IPM Lab. (2011).

[7] http://www.apr1400.com.

[8] J. Sigrist, D. Broc, and C. Laine, "Dynamic analysis of a nuclear reactor with fluid structure interaction: part 1. seismic loading, fluid added mass and added stiffness effects," *Nucl. Eng. Des*., vol. 236, pp. 2431-2443 (2006)

[9] R. G. Dong, "Effective mass and damping of submerged structures," California Univ., Livermore, Lawrence Livermore Lab. (1978).

[10] M. K. Kwak, "Vibration of circular plates in contact with water," *J. Appl. Mech*., vol. 58(2), pp. 480–483 (1991).

[11] M. K. Kwak and K. C. Kim, "Axisymmetric vibration of

circular plates in contact with fluid," *J. Sound Vib*., vol. 146(3), pp. 381–389 (1991).
[12] F. Zhu, "Rayleigh quotients for coupled free vibrations," *J. Sound Vib*., vol. 171, pp. 641–649 (1994).
[13] F. Zhu, "Rayleigh–Ritz method in coupled fluid–structure interesting systems and its applications," *J. Sound Vib*., vol. 186, pp. 543–550 (1995).
[14] M. Amabili, M. Frosali, and M. K. Kwak, "Free vibrations of annular plates coupled with fluids," *J. Sound Vib*., vol. 191(5), pp. 825–846 (1996)